J. Marine Sci. Appl. (2017)16
DOI: 10.1007/s11804-017-1389-7

Effect of WO_3 Nanoparticle Loading on the Microstructural, Mechanical and Corrosion Resistance of Zn Matrix/TiO_2-WO_3 Nanocomposite Coatings for Marine Application

A. P. I. Popoola[1], A. A. Daniyan[2, 3], L. E. Umoru[2] and O. S. I Fayomi[1, 4*]

1. Department of Chemical, Metallurgical and Materials Engineering, Tshwane University of Technology, Pretoria 0001, South Africa
2. Department of Materials Science and Engineering, Obafemi Awolowo University, Ile-Ife, Nigeria
3. Engineering Materials Development Institute, P.M.B 611, Akure, Nigeria
4. Department of Mechanical Engineering, Covenant University, P.M.B 1023, Ota, Ogun State, Nigeria

Abstract: In this study, for marine application purposes, we evaluated the effect of process parameter and particle loading on the microstructure, mechanical reinforcement and corrosion resistance properties of a Zn-TiO_2-WO_3 nanocomposite produced via electrodeposition. We characterized the morphological properties of the composite coatings with a Scanning Electron Microscope (SEM) equipped with an Energy Dispersive Spectrometer (EDS). We carried out mechanical examination using a Dura Scan hardness tester and a CERT UMT-2 multi-functional tribological tester. We evaluated the corrosion properties by linear polarization in 3.5% NaCl. The results show that the coatings exhibited good stability and the quantitative particle loading greatly enhanced the structural and morphological properties, hardness behavior and corrosion resistance of the coatings. We observed the precipitation of this alloy on steel is greatly influenced by the composite characteristics.
Keywords: Zn-TiO_2-WO_3, Nanocomposite, Nanoceramics, coatings matrix and precipitation

1 Introduction

When materials are reduced to the nanoscale, they display special properties that differ significantly from those exhibited in the bulk state, soft materials become hard, opaque materials become transparent, insulators turn to conductors, inert materials become reactive and dielectrics becomes conductors (Afonja, 2009 ; Daniyan *et al*., 2014).

Nanocomposite materials have various unique properties, including excellent corrosion and wear resistance, resistance to high temperature oxidation, self-lubricity and so on (Ger and Grebe, 2004) Coating via electrodeposition have been considered to be one of the most viable techniques for fabricating nanocomposite because of its low temperature operation, precise control, high rate of deposition and cost effectiveness (Praveen and Ventekatesha, 2011). Zn coated materials are characterized by high corrosion resistance in aggressive environment and the corrosion resistance of zinc coatings can be significantly enhanced by Zn-based composite (Rahman *et al*., 2009). Several authors have reported that ZrO_2, TiO_2, Al_2O_3 and SiC particulates could be co deposited with metals or metallic alloys to form composite coatings (Rahman *et al*., 2009; Panek *et al*., 2011; Wang *et al*., 2011). Similarly, some alloys and composites such as Ni-W, Zn-ZrO_2 and Ni-W-SiC are currently being developed as surface treatment substitutes for chromium coatings because of their excellent performance and environmental friendliness.

A number of researchers have studied WO_3 as an incorporation particulate for composite reinforcement; but the use of nanosized WO_3 for composite strengthening has received little attention. In this study we prepared and electrodeposited TiO_2-WO_3 in a Zn matrix on mild steel substrates, which readily corroded in a chloride bath. We investigated the effect of particulates loading of WO_3 particulate loading on themicrostructural, mechanical reinforcement and corrosion resistance properties of a Zn matrix/TiO_2-WO_3 nanocomposite coating.

2 Experimental procedure

The experimental procedure for the coatings, their characterization and corrosion studies are being described.

2.1 Preparation of substrate

We used a mild steel (substrate) sheet with the dimensions 45 mm×40 mm×20 mm and prepared zinc sheets 85 mm× 45 mm×5 mm as anodes. Table 1 shows the chemical composition of the mild steel specimens. The cathode was a mild steel coupon and the anode was commercial pure zinc (99.99%). We mechanically polished the mild steel specimens, then degreased and rinsed them with water as described in (Popoola and Fayomi, 2011; Fei *et al.*, 2006).

2.2 Formation of deposited coating

We activated the mild steel substrate prepared earlier by dipping it into 10% HCl solution for a few seconds followed by rinsing in deionized water. We used Analar-grade

Received date: 10-Jan-2016
Accepted date: 21-Sep-2016
***Corresponding author Email:** ojosundayfayomi3@gmail.com

chemical sand deionized water to prepare the plating solution at room temperature before plating. We prepared the bath formulations the previous day and, to obtain homogeneous solution, stirred continuously at 400 r/min with constant heating at 70 °C throughout the plating process. We maintained the pH at 4.5 to achieve good deposition. We used the following bath compositions for the different coating matrixes: $ZnCl_2$ 120 g/L, KCl 30 g/L, TiO_2 nanoparticles 20 g/L, WO_3 nanoparticles 8–15 g/L, 2-butyne 1, 4 diol 0.5 g/L, cetylpridinium chloride 0.5 g/L, and 10 g/L thiourea.

Our choice of the deposition parameter is in line with the previous work of some of our group (Fayomi *et al.*, 2014). We connected the prepared zinc electrodes to the rectifier at varying currents between 1.0 and 1.5 A for 20 min. We then rinsed the coated samples in water and air dried them. Thereafter, we segmented pieces of the coated steel for characterization. Tables 1 and 2 show the formulation-designed bath composition for the Zn-TiO_2-WO_3 nanocomposite and the electrodeposition parameters with results for the coated mild steel, respectively. The significant increase in the coating thickness and weight is a function of the addition of mass, the current density, and other deposition parameters that may typically influence the surface properties (Fayomi *et al.*, 2014).

Table 1 Chemical composition of the mild steel used in the study

Element	% Content	Element	% Content	Element	% Content
C	0.328	Mo	0.096	Ti	0.035
Si	0.873	Ni	0.031	V	0.009
Mn	0.431	Cu	0.113	W	0.006
P	<0.003	Al	0.033	B	<0.002
S	>0.156	Co	0.032	Sn	0.0014
Cr	0.103	Nb	0.014	Fe	99.61

Table 2 Electrodeposition parameters and results for the coated mild steel

Sample	Time/min	Coating thickness/μm	Weight gained/g	Current/A	Coating per unit area/(g·cm^{-2})
Zn-TiO_2-WO_3-8g-1.0A	20	25	0.45	1.0	0.024
Zn-TiO_2-WO_3-8g-1.5A	20	60	0.48	1.5	0.030
Zn-TiO_2-WO_3-15g-1.0A	20	35	0.41	1.0	0.023
Zn-TiO_2-WO_3-15g-1.5A	20	40	0.51	1.5	0.036

2.3 Characterization of coating

We characterized the obtained nanocomposite coatings with a JEOL Field Emission JSM–7600F Scanning Electron Microscope (SEM) equipped with an Energy Dispersive Spectrometer (EDS). We used X-ray powder diffraction (XRD) to study the structural composition. We used Diamond pyramid indenter EMCO Test Dura-scan 10 micro-hardness testers to conduct microhardness evaluations at a load of 10 g for a period of 20 s. We measured the micro-hardness across the plated surface.

2.4 Wear tests

As shown in the schematic diagram in Fig. 1, we characterized the tribological properties of the composite coating using a CERT UMT-2 multi-functional tribological tester at an ambient temperature of 25 °C. We carried out reciprocating sliding tests with a load of 5 N, a constant speed of 5 mm/s, and displacement amplitude of 2 mm for 20 min. We chose a Si3N ball (4 mm in diameter, HV 50g-1600) as a counter body for our examination of the tribological behavior of the coated sample. As prescribed by the specimen holder, the wear specimen dimensions were 2cm by 1.5 cm. After the wear test, we further examined the structure of the wear scar and the worn tracks of the film with a high optics Nikon Optical Microscope (OPM) and the JEOL Field Emission SEM/EDS.

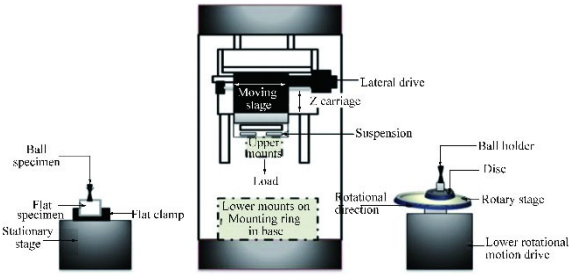

Fig. 1 Schematic view of reciprocating sliding friction CERT UMT-2 test system (Fayomi *et al.*, 2014)

2.5 Electrochemical test

We performed electrochemical studies with an Autolab PGSTAT 101 Metrohm Potentiostat using a three-electrode cell assembly in a 3.5% NaCl static solution at room temperature. We used the developed composite as the working electrode and a platinum electrode as the counter electrode. We evaluated the corrosion rate with the attached software, which had built-in formulas in accordance with the Stern-Geary and Faraday laws of electrolysis.

$$I_{\text{corr}} = \frac{1}{R_p} \frac{\beta_a \beta_c}{2.303\left(\beta_a + \beta_c\right)} \tag{1}$$

Modifying Eq. (1) with Faraday law,

$$CR = \frac{i_{corr} K \cdot EW}{d} \quad (2)$$

where i_{corr} is the corrosion current density in A/m^2, K is a constant that defines the units for the corrosion rate, EW is the equivalent weight in grams/equivalent, d is density in g/cm^3, β_a and β_c are Tafel slopes of the anodic and cathodic reactions respectively.

3 Results and discussion

3.1 Morphological studies

Figs. 2–4 show the SEM/EDS structure of Zn-TiO_2-WO_3-8g-1.0A and Zn-TiO_2-WO_3-15g-1.5A nanocomposite matrices respectively, as fabricated on mild steel. From Figs. 3 and 4, we can see that the crystallite nodules of the deposits were homogeneously distributed on the interface. We also clearly observed that with 8 g of WO_3 nanoparticles, there was a noticeable crystallite of the composite nodules along the interface. Actually, there are two distinct phases, the first having a homogeneously identical steady precipitate and the latter exhibiting hexagonal agglomerate patches. Clearly, the incorporation of the WO_3 along the zinc interface could indicate the refined morphology of the fine nodular particles. Moreover, from Fig. 5, the incorporation of the TiO_2 along the WO_3 in the zinc interface could indicate the refined morphology of fine spherical/nodular particles, as compared with the flake-like Zn particles. Fig. 6 shows SEM images of the coatings at higher magnification and further reveals their morphologies in the nano range.

The plated appearance and coating interface of the Zn-TiO_2-WO_3 were gratifying because the nano ceramic particulates fortified the composite in the zinc metal matrix. The structural performance was enhanced as expected since the nucleation process was initiated from the zinc metal as load carrier, and the distribution of the particulate covered the nucleation spot and strengthened the produced composite (Fayomi *et al.*, 2014; Umoru *et al.*, 2006; Wang *et al.*, 2011). Furthermore, we note that the microstructural change may be due to the higher particle loading of the WO_3 nanoceramic composite leading to better precipitation and enhanced orientation. Also, according to (Wang *et al.*, 2011), the conditioning factor with respect to the quantity of additive can also play a very important role in modifying the crystal direction and surface quality of a deposited material.

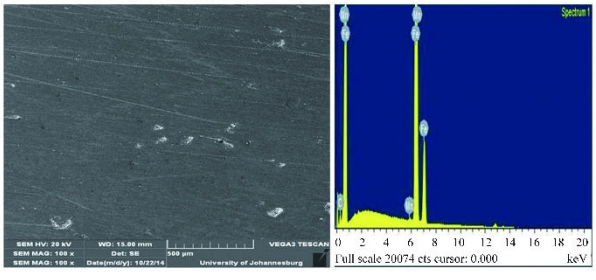

Fig. 2 SEM/EDS spectra of as-received mild steel

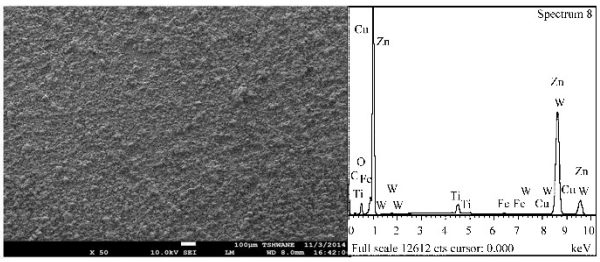

Fig. 3 SEM/EDS of Zn-TiO_2-WO_3-8g at 1.0 A coated mild steel showing the surface morphology

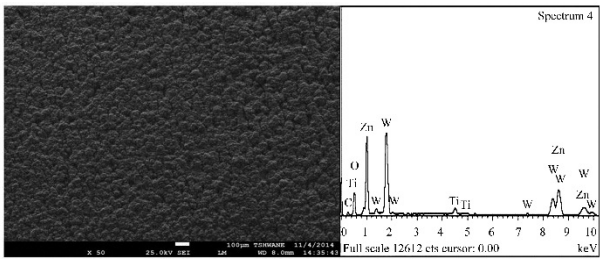

Fig. 4 SEM/EDS of Zn-TiO_2-WO_3-15g at 1.5 A coated mild steel showing the surface morphology

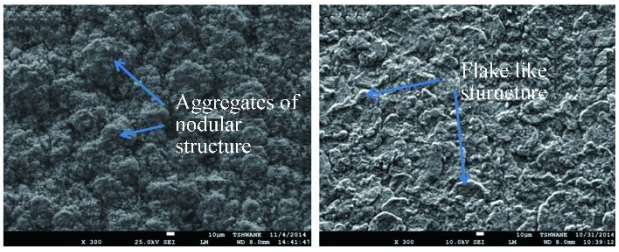

(a) Zn-TiO_2-WO_3 (b) Zn coated mild steel

Fig. 5 SEM/EDS of Zn-TiO_2-WO_3 and Zn coated mild steel showing the internal morphology of the coatings

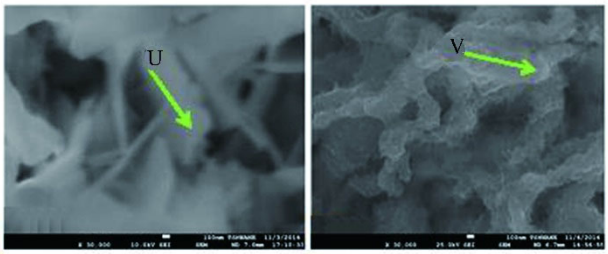

Fig. 6 SEM/EDS of (a) and (c) Zn-TiO_2-WO_3-8g-1.0A (b) and (d) Zn-TiO_2-WO_3-15g-1.5A- coated mild steel showing the internal morphology of the coatings at the nanolevel- 100 nm ('U' and 'V' are Zn-TiO_2-WO_3– rich portions)

3.2 Microhardness evaluation

The microhardness evaluation in Fig. 7 shows the effect of the composite microstructure and its particle loading on the hardness behavior of the Zn-TiO_2-WO_3 nanocomposite coatings.

Generally, all the produced nanocomposites display excellent and unique improvement compared to the unplated mild steel substrate, which can be traced to the effect of the

WO_3 nanosized particulate loading. However, the sample matrix Zn-TiO_2-WO_3-15g-1.0A exhibited the highest hardness property. The outstanding enhancement of this matrix is primarily due to microstructural strengthening from the increased quantity of WO_3 loaded into the Zn-TiO_2 matrix, although the hardness decreased as the supplied current was increased from 1.0 A to 1.5 A. This reduction in hardness could have been influenced by the anomaly that occurs in Faraday's first law of electrolysis. Factors such as the operating conditions, electrolyte composition, and mechanism of diffusion could also influence the result (Popoola *et al*., 2012; Fayomi *et al.*, 2014). Figs. 8–10 show the response of the composite coating to heat treatment. We observed thermal deformations after 250 °C for 5 h and we investigated the mechanical responses of the coated samples. Although heating did not increase the hardness properties of all the samples, neither did the coatings experience any cracks or flaws at the interface, but rather a kind of grain refinement, as can be seen in Fig. 11. Furthermore, Fig. 12 illustrates the change in granularity of the nanocomposite and zinc coating surfaces obtained by optical micrographs. We can see that annealing at a temperature of 500 °C completely recrystallized the grains of the nanocomposite. This thermal treatment facilitates improved crystallization. The thermally attacked surfaces of the Zn–coated surface could be due to the fact that the annealing treatment was carried out at 500 °C which is appreciably higher than 419.5 °C (melting point of Zn). In contrast, the synergistic effect of the WO_3 and TiO_2 nanoparticulate mitigated this effect in the nanocomposite- coated steel. Due to the thermal treatment and the porosity of the alloy surface, the mechanical behavior could result in a hardness distribution. Some studies also agree that compression stress could significantly increase the microhardness when it is much less than the ultimate strength of the coating. However, Paunovic and Mordechay (2006) revealed that for flaws such as porosity, the macroparticles at the alloy surface will have unfavorable effects on the mechanical properties. Figs. 9 and 10 compare the hardness properties of the composite coatings before and after thermal treatment, respectively. The average microhardness values for all the calculated samples indicate that Zn-TiO_2-WO_3-15g-1.0A nanocomposite coatings possessed the highest hardness value of 237.5 HVN, which increased to 250 HVN after heat treatment and then maintained this optimal value. We can also deduce from Fig.10 that, the hardness after heat treatment increased from 139 HVN to 145.5 HVN and 188.5 to 145 HVN when the mass of WO_3 increased from 8 g to 15 g respectively, but decreased from 188.5 to 145 HVN and 153 to 137 HVN as the current increased from 1.0 to 1.5 A, respectively, with increased WO_3 particle loading, and decreased with increases in the input current. The performance of the coatings was excellent since the hardness values after heating maintained more than 50% of their values before thermal treatment (Chin and Nobe, 1972). We also observed the phenomenon of dispersion strengthening. The mechanism soft this strengthening include grain refinement strengthening and dispersion strengthening by the WO_3 deposited on the sample and the deposition current (Kwok *et al.*, 2006; Fayomi *et al*., 2016).

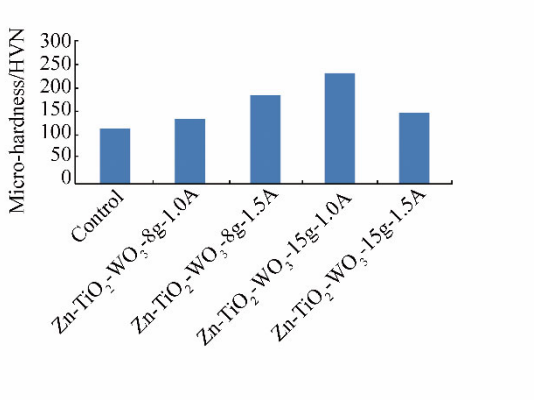

Fig. 7 Hardness properties at different currents of Zn-TiO_2-WO_3 nanocomposite deposited on mild steel before heat treatment

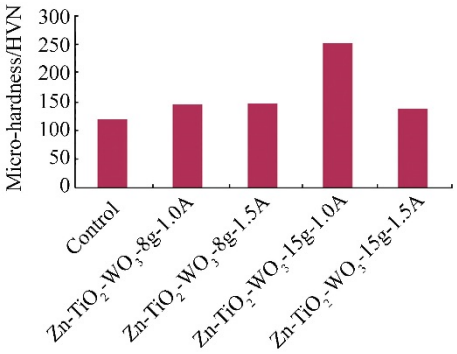

Fig. 8 Hardness properties at different currents of Zn-TiO_2-WO_3 nanocomposite deposited on mild steel after heat treatment

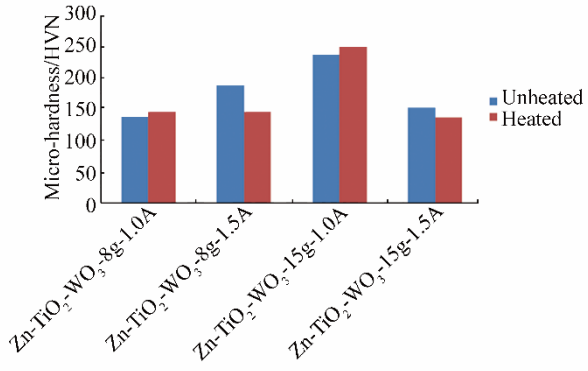

Fig. 9 Microhardness variation of the nanocomposite coating before and after heat treatment

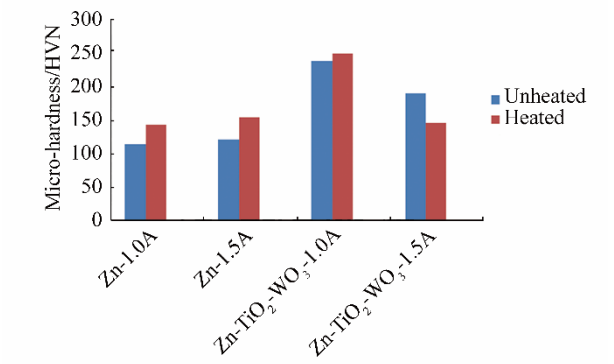

Fig. 10 Microhardness variation of the zinc and nanocomposite coating before and after heat treatment

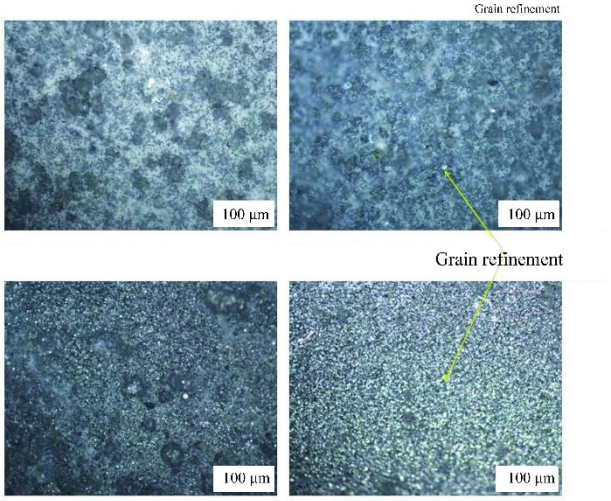

Fig. 11 Optical micrographs (a) and (b) Zn-TiO2-WO3-8g-1.0A nano-composite coating before and after thermal treatment, respectively, and (c) and (d) Zn-TiO2-WO3-15g-1.5A nano-composite coating before and after thermal treatment

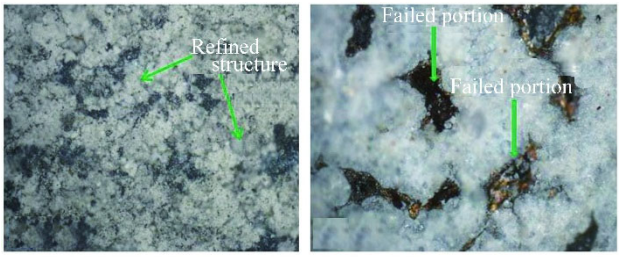

(a) Zn-TiO_2-WO_3 coated steel (b) Zn coated steel

Fig. 12 OPM micrographs after annealing at 500 °C

3.3 Wear analysis of the composite coating on mild steel

Figs. 13 and 14 show the wear loss of the Zn coating and different sample matrices of the Zn-TiO_2-WO_3 nanocomposite coating. The wear resistances of the nanocomposite coatings were obviously greater than that of the control (unplated sample) and even more than that of the Zn coating. It is evident that the wear loss decreases with increases in the current and particle loading until 15 g of WO_3 is loaded at 1.5 A. Thus the wear resistance of the composite coatings increases with increases in the WO_3 nanoceramic content, as revealed by that fact that Zn-TiO_2-WO_3-15g-1.0A displayed the optimum wear resistance, but the addition of WO_3 to the matrix contributed greatly to the wear resistance. This can be attributed to the strengthening effect of the WO_3 particle loading. The hardness process parameter and microstructural behavior are the parameters that affect the wear resistance (Popoola and Faypmi, 2011; Noor and Al-Moubaraki, 2008). The wear resistance increases with increasing matrix hardness.

The plastic deformation tendency of Zn-TiO_2-WO_3-15g-1.0A nanocomposite coatings is the least. These results suggest that the wear resistance was improved by the addition of WO_3 particles. According to Popoola and Fayomi (2011), the embedded WO_3 particles can significantly improve the tribological performance of Zn-TiO_2-WO_3 nanocomposite coatings.

Fig. 15 shows the microscopic image of worn surfaces of the coated samples of Zn-TiO_2-WO_3 at varying WO_3 nanoparticle loading levels and different input currents. From the scar, we can see plastic deformation and grooves on the sample surfaces. The reciprocating sliding disc had a high impact on the substrates and we can see that penetration resulted in stress through minor fractures. The coated sample with Zn-TiO_2-WO_3-15g-1.0A displayed the best appearance, had the least visible plastic deformation, and exhibited a unique network of worn tracks that are consistent with the results in Fig. 9. Clearly, the embedded conditioned composite matrix could have been responsible for this wear resistance, especially in the presence of TiO_2 and WO_3.

Shibli *et al.* (2010) reported in their review on composite studies that mixed oxide can provide excellent wear resistance properties. In view of this, undetected plastic deformation from composite coatings is a strong early indication of the development of oxide films on the worn surfaces of composites that provide a higher wear resistance, as expected.

We note that no serious fracture occurred in any of the samples. Moreover, the continuous decrease in the coefficients of friction during the wear mechanism may decrease the severity of the plastic deformation of the samples, and Zn-TiO_2-WO_3-15g-1.0A showed the lowest coefficients of friction, in accordance with (Fayomi and Popoola, 2013).

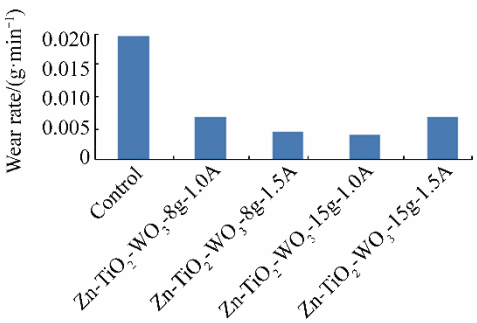

Fig. 13 Variation of wear rate of Zn-TiO_2-WO_3 coatings and uncoated steel with time

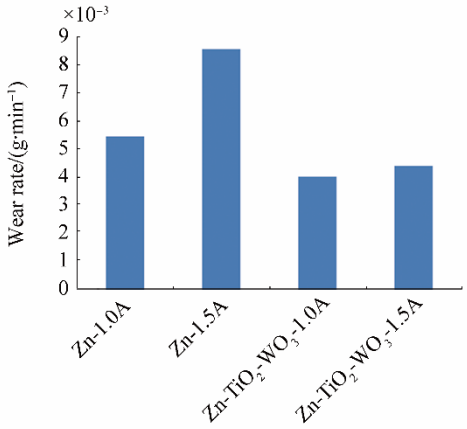

Fig. 14 Variation of wear rate of Zn-TiO_2-WO_3 and Zn coated steel with time

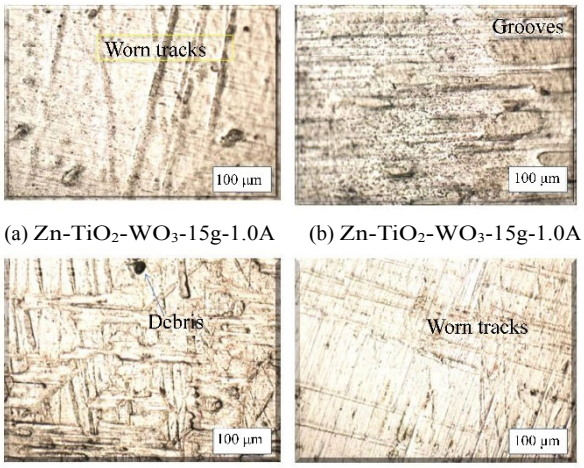

(a) Zn-TiO_2-WO_3-15g-1.0A (b) Zn-TiO_2-WO_3-15g-1.0A

(c) Zn-TiO_2-WO_3-15g-1.0A (d) Zn-TiO_2-WO_3-15g-1.0A

Fig. 15 OPM micrograph of the wear scar for chloride deposited samples

3.5 Polarization measurements

As presented in Table 3, we extrapolated the E_{Corr}, I_{Corr}, Corrosion Rate (CR), and polarization resistance (R_P) values of the samples from the Tafel slope. The results indicate the corrosion resistance behavior of the coatings in 3.5% NaCl static solution. From the polarization curves of the Zn-TiO_2-WO_3 composite coating in Fig. 16, we found that the addition of WO_3 altered the shape of the polarization curve but caused a considerable increase in the E_{corr} value. These characteristics indicate that an increase in additive concentration enhances this process. However, the optimal value for the coating with the least corrosion rate was Zn-TiO_2-WO_3-15g-1.5A, which implies that the addition of WO_3 provides a better corrosion resistance effect. According to Ogundare *et al.* (2012), Fayomi *et al.* (2016), this could be attributed to the nature and tenacity of the passive film produced by Zn-TiO_2-WO_3-15g-1.5A on the surface of the coated steel. Clearly, there was appreciable improvement in the potential for all coatings, which could be attributed to the coating effect of the film precipitated at the interface of the Zn matrix. Substrates that form less passive films on the surface results in severe corrosion attack by chloride solutions having a potential of about −1.4 V, which is below that of the coated samples. The coating properties of all the coatings were excellent. Table 2 shows a summary of the polarization measurement results, which we obtained from Tafel plots. The drop in the potential thereafter could be traced to a slight passivity breakdown when the concentration of WO_3 was further increased Fayomi *et al.* (2015) (Su and Kao, 2011). Figs. 17–19 show the morphologies of the composite coating before and after the corrosion tests in the accelerated solution. Uniform and localized corrosion occurred on the mild steel substrate while we observed only uniform corrosion on all the surfaces of the Zn-TiO_2-WO_3 series. TiO_2-rich intermetallic particles and excess WO_3 globules form pit initiation sites and promote cathodic reduction reactions.

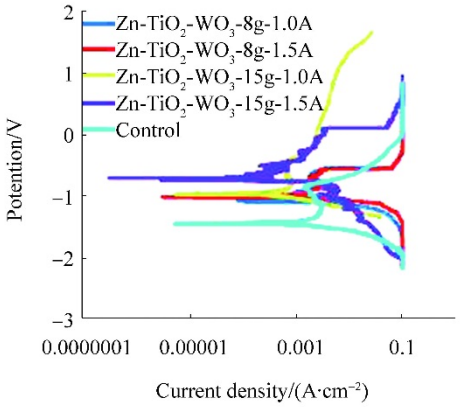

Fig. 16 Potentiodynamic polarization curves of Zn-TiO_2-WO_3 composite coating on mild steel in 3.5% NaCl solution

Table 3 Polarization data extrapolated from Tafel slope for matrix Zn-TiO_2-WO_3 composite coating

Sample in 3.5% NaCl	E_{corr}/V	i_{corr} (A·cm^{-2})	Corrosion rate (mm·a^{-1})	Polarization resistance/Ω
Control	−1.439 21	0.005 083	1.956 6	18.037
Zn-TiO_2-WO_3-8g-1.0A	−1.071 78	0.001 485	0.571 74	31.54
Zn-TiO_2-WO_3-8g-1.5A	−1.007 39	0.001 226	0.471 82	35.521
Zn-TiO_2-WO_3-15g-1.0A	−0.968 628	0.000 934	0.359 64	41.524
Zn-TiO_2-WO_3-15g-1.5A	−0.704 62	0.000 263	0.101 16	99.428

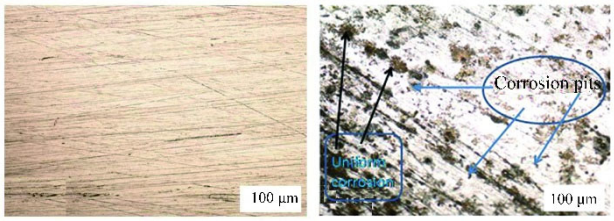

(a) Before corrosion (b) After corrosion

Fig. 17 Optical micrographs of the uncoated (control) samples

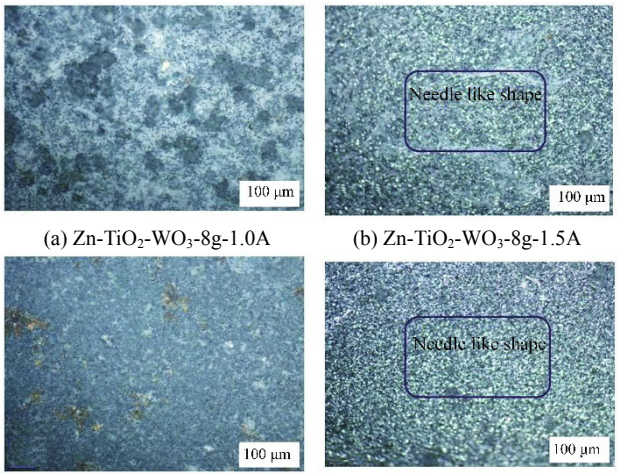

(a) Zn-TiO_2-WO_3-8g-1.0A (b) Zn-TiO_2-WO_3-8g-1.5A

(c) Zn-TiO_2-WO_3-15g-1.0A (d) Zn-TiO_2-WO_3-15g-1.5A

Fig. 18 Optical micrographs of the nano-composite coating before corrosion

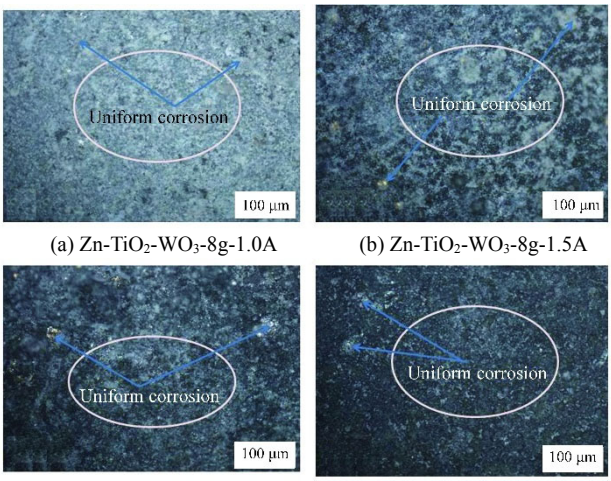

(a) Zn-TiO_2-WO_3-8g-1.0A (b) Zn-TiO_2-WO_3-8g-1.5A

(c) Zn-TiO_2-WO_3-15g-1.0A (d) Zn-TiO_2-WO_3-15g-1.5A

Fig. 19 Optical micrographs of the nano-composite coating after corrosion

4 Conclusions

1) We used nanostructured WO_3 particulates to generate Zn-TiO_2-WO_3 composite coatings from a chloride bath.

2) We used EDX to confirm the incorporation of WO_3 in the coating

3) Higher corrosion potential, higher microhardness, and higher wear resistance of the nanocomposites was associated with higher corrosion resistance than that of the uncoated substrate.

4) The incorporation of the TiO_2/WO_3 nanoceramic composite particles in the zinc matrix as reinforcement enhances the hardness properties of the substrate. The hardness properties increase with increases in the additive concentration.

5) The improvement in the corrosion resistance may be due to the physical barriers produced by WO_3 to the corrosion process by filling crevices and minute holes on the surface of the composite coating.

Acknowledgement

This work is based upon the financial support of National Research Foundation and effort by the Surface Engineering Research Centre (SERC), Department of Chemical Metallurgical and Materials Engineering, the Tshwane University of Technology, Pretoria, South Africa. The privilege given by Department of Materials Science and Engineering, Obafemi Awolowo University to undertake this research work is also appreciated.

References

Afonja AA, 2009. Novel materials for energy applications. *Nigerian Journal of Materials Science and Engineering*, **1**(1), 63-72.

Chin RJ, Nobe K, 1972. Electrodissolution kinetics of iron in chloride solutions. *J. Electrochem. Soc.*, **119**(11), 1457-1461.

Daniyan AA, Umoru LE, Fasasi AY, Borode JO, Oluwasegun KM, Olusunle SOO, 2014. Electrical properties of Nano-TiO_2 thin film using spin coating method. *Journal of Minerals and Materials Characterization and Engineering*, **2**, 15-20. DOI: 10.4236/jmmce.2014.21003

Fayomi OSI, Aigbodion VS, Popoola API, 2015. Properties of Tic/Tib modified Zn–Tic/Tib ceramic composite coating on mild steel. *Journal of Failure Analysis and Prevention*, **15**(1), 54-64. DOI: 10.1007/s11668-014-9908-1

Fayomi OSI, Joseph OO, Mubiayi MP, Durodola BM, Gabriel O, 2016a. Microstructural evolution and characterization of super-induced MgO composite on zinc-rich coating. *Egyptian J. of Basic and Appl. Sci.*, **3**(1), 1-9. DOI: 10.1016/j.ejbas.2015.05.007

Fayomi OSI, Loto CA, Popoola API, Tau V, 2014a. Effect of process parameter on the in-situ intermetallic composite coating and microstructural evolution of Zn-Al_2O_3 in the presence of TEA/MEA on mild steel. *Int. J. Electrochem. Sci.*, **9**, 7359-7368.

Fayomi OSI, Popoola API, Adams FV, 2016b. Evolution and anticorrosion properties of ni-cu thin film coatings on low carbon steel. *Asian Journal of Chemistry*, **28**(1), 129. DOI: 10.14233/ajchem.2016.19270

Fayomi OSI, Popoola API, Aigbodion VS, 2014b. Effect of thermal treatment on the interfacial reaction, microstructural and mechanical properties of Zn-Al-SnO_2/TiO_2 functional coating alloys. *Journal of Alloys and Compounds*, **617**, 455-463. DOI: 10.1016/j.jallcom.2014.07.141

Ger MD, Grebe R, 2004. Electrochemical deposition of nickel/SiC composites in the presence of surfactants. *Materials Chemistry and Physics*, **87**(1), 67-74.

DOI: 10.1016/j.matchemphys.2004.04.022

Kwok CT, Cheng FT, Man HC, 2006. Cavitation erosion and corrosion behaviours of laser-aluminized mild steel. *J Surf Coat Technol*, **200**(11), 3544-3552.
DOI: 10.1016/j.surfcoat.2004.12.016

Noor EA, Al-Moubaraki AH, 2008. Corrosion behavior of mild steel in hydrochloric acid solutions. *Int. J. Electrochem. Sci*., **3**, 806-818.

Ogundare O, Babatope B, Adetunji AR, Olusunle SOO, 2012. Atmospheric corrosion studies of ductile iron and austenitic stainless steel in an extreme marine environment. *Journal of Minerals and Materials Characterization and Engineering*, **11**, 914-918.

Panek J, Bierska-Piech B, Karolus M, 2011. The corrosion resistance of zinc-nickel composite coatings. *Journal of Achievements in Materials and Manufacturing Engineering*, **45**(2), 157-162.

Paunovic M, Mordechay S, 2006. *Fundamentals of electrochemical deposition*. 2nd ed, John Wiley and Son Inc., University of Windsor, Windsor, **6**, 388-391.

Popoola API, Fayomi OSI, 2011. ZnO as corrosion inhibitor for dissolution of zinc electrodeposited mild steel in varying HCl concentration. *Int. J. of the Phy. Sci*., **6**, 2447-2454.

Popoola API, Fayomi OSI, Popoola OM, 2012. Comparative studies of microstructural, tribological and corrosion properties of plated Zn and Zn-alloy coatings. *International Journal of Electrochemical Science*, **7**, 4860-4870.

Praveen BM, Venkatesha TV, 2011. Electrodeposition and corrosion resistance properties of Zn-Ni/TiO_2 nano-composite coatings. *International Journal of Electrochemistry*, 1-4.

Rahman MJ, Sen SR, Moniruzzaman M, Shorowordi KM, 2009. Morphology and properties of electrodeposited Zn-Ni alloy coatings on mild steel. *Journal of Mechanical Engineering*, **40**(1), 9-14.

Shibli SMA, Chacko F, Divya C, 2010. Al_2O_3–ZrO_2 mixed oxide composite incorporated aluminium rich zinc coatings for high wear resistance. *Journal Corrosion Science*, **52**(2), 518-525.
DOI: 10.1016/j.corsci.2009.10.008

Shivakumara S, Manohar U, ArthobaNaik Y, Venkatesha TU, 2007. Influence of additives on electro-deposition of bright Zn-Ni alloy on mild steel from acid sulphates bath. *Bull Mater Sci*, **30**, 455-462.

Su YL, Kao WH, 2011. Tribological behaviour and wear mechanism of MoS_2–Cr coatings sliding against various counter body. *Tribol*ogy Inter*national*, **36**(1), 11-23.
DOI: 10.1016/S0301-679X(02)00095-6

Umoru LE, Fawehinmi IA, Fasasi AY, 2006. Investigation of the inhibitive influence of theobroma cacao and cola acuminata leaves extracts on the corrosion of mild steel in sea water. *Journal of Applied Sciences Research*, **2**(4), 200-204.

Wang P, Cheng Y, Zhang Z, 2011. A study on the electrocodeposition processes and properties of Ni-SiC nanocomposite coating. *Journal of Coatings Technology and Research*, **8**(3), 409-417.
DOI: 10.1007/s11998-010-9310-1